Electron Backscatter Diffraction Study on Microstructure, Texture, and Strain Evolution in Armco Iron Severely Deformed by the Differential Speed Rolling Method

WOJCIECH POLKOWSKI, PAWEŁ JÓŹWIK, and ZBIGNIEW BOJAR

Results of the electron backscatter diffraction (EBSD) study on structural changes in Armco iron subjected to severe plastic deformation by differential speed rolling (DSR) with different values of roll speed mismatch (R = 1, 2, 3, and 4) are shown in the present article. Results of the EBSD microstructure evaluation reveal that a differentiation of roll speeds results in an effect of structure refinement—iron samples processed with high roll speed mismatch are characterized by a high fraction of grains with submicron size. A microtexture examination shows that the DSR process leads to an overall texture weakening effect and a displacement (a shifting to different ''stable'' positions) of the basic rolling texture components, due to an additional presence of a simple shear component in the deformation gradient imposed to the material. Despite the higher hardness of the DSR-processed samples, results of the EBSD strain analysis indicate that some part of the stored deformation energy is released during rolling with an additional presence of shear strain. This finding points toward the possibility of activating a dynamic transformation of the material structure into some more stable state. However, since the observed structural changes take place inside deformation bands and do not lead directly to the formation of a fully equiaxed grain structure, it seems to be more reasonable to call the observed structure transformation a subgrain structure evolution through accumulated shear deformation, which may be related to the dynamic recovery process.

DOI: 10.1007/s11661-015-2760-4

I. INTRODUCTION

THE processing and properties of ultrafine-grained (UFG) materials have generated considerable interest recently from both an industrial and a scientific standpoint. The impact of structure refinement to a submicron level on the substantial improvement of mechanical and performance properties of structural materials has been generally established.[1] UFG metals and alloys exhibit extremely good mechanical properties characterized by high mechanical strength and good ductility,[2]] as well as a possibility of superplastic forming at low temperature.[3] Furthermore, a large fraction of high-angle grain boundaries (HAGBs) in a volume of bulk material is a key factor in the faster kinetics of diffusion-based phenomena leading to, *e.g.*, better corrosion resistance of UFG materials, as compared to their coarse-grained counterparts.[4]

Severe plastic deformation (SPD) methods are one of the most efficient ways to produce bulk UFG metals. In these techniques, an extremely high strain is imposed on a material in order to obtain the structure refinement effect through formation of intersected shear bands[5] or a dynamically activated recovery or recrystallization process.[6]

So far, there are a few hydrostatic SPD methods that have been successfully used to fabricate UFG metals and alloys (*e.g.*, equal channel angular pressing, cyclic extrusion compression, or high pressure torsion). These and other methods were described recently in a comprehensive review article by Estrin and Vinogradov.[7] However, despite positive results in terms of structure and properties control, hydrostatic SPD techniques have rather poor industrial potential due to the small size of processed samples and low manufacturing efficiency. Thus, development of SPD methods that are based on highly efficient, continuous plastic deformation processes has generated considerable research interest.

In recent years, some new SPD methods based on modified conventional manufacturing processes have been proposed. Differential speed rolling (DSR) is a modification of the rolling process that includes an application of different values of rotational speed for upper and lower rolls. An implementation of asymmetry of the rolling gap leads to an imposition of a high through thickness shear strain to the material. As a consequence of the change of the deformation gradient, the effects of both higher accumulated strain and quantitative/qualitative alteration of crystallographic texture, compared to a normal rolling process, are observed. Furthermore, due to the continuous character of the rolling process, the DSR method may be easily

WOJCIECH POLKOWSKI, Master's Student, PAWEŁ JÓŹWIK, Postdoctoral Student, and ZBIGNIEW BOJAR, Professor, are with the Department of Advanced Materials and Technologies, Faculty of Advanced Technologies and Chemistry, Military University of Technology, Gen. S. Kaliskiego 2 St., 00-908 Warsaw, Poland. Contact e-mail: wpolkowski@wat.edu.pl

Manuscript submitted September 1, 2014.
Article published online February 18, 2015

adopted to large scale industrial processing of materials. DSR has been widely analyzed as a tool of strain-induced microstructure refinement and as a method of crystallographic texture modification (and, thus, an improvement of anisotropy in the mechanical properties of rolled products).

The grain refinement effect by the DSR method was previously observed in numerous pure metals and alloys. Results reported by Zuo *et al.*[8] show that very fine grains, 50 nm in size, are obtained in pure aluminum through cold rolling with differentiation of roll speed. Furthermore, experimental results described by Kim *et al.*[9] revealed that commercially pure titanium subjected to a combination of warm and cold DSR processes is characterized not only by an UFG structure and high strength but also by superior corrosion resistance, with the corrosion rate in acid solutions almost two times lower than that of coarse-grained material. Additionally, in the case of precipitation-strengthened AZ91Mg-based alloy, an application of DSR results in both an ultrafine grain size (~300 nm) and more uniform distribution of strengthening particles upon postdeformation low-temperature aging treatment.[10] The results of our previous study on commercially pure copper[11] also point out that a shear strain imposed during rolling with different values of roll velocity allows obtainment of material with grain size in the submicron range and a high fraction of HAGBs, indicating dynamic transformation of the microstructure. Moreover, we recently showed that the DSR method also may be successfully applied to improvement of mechanical properties of hardly deformable materials such as intermetallic-based alloys.[12]

Despite the limited reported data, similar results were also presented in a few articles on the DSR-processed low carbon steel. Suharto and Ko[13] reported that the initial ferrite grain size of 35 μm was significantly refined to 700 nm after DSR processing under the roll speed ratio of 1:4 for lower and upper rolls. An even greater effect of grain refinement (to 500 nm) was presented in the recent work of Hamad *et al.* on interstitial-free (IF) steel subjected to DSR operations.[14] Additionally, these authors concluded that the finest and most uniform grain structure was obtained when a high value of reduction per pass was applied in the DSR process.

As previously mentioned, the DSR process was also successfully applied in the field of controlling the crystallographic texture of engineering materials. This issue is especially important for aluminum and magnesium alloys, which, due to formation of unfavorable rolling and recrystallization textures, possess a worse susceptibility to deep drawing than widely applied low carbon steels. However, it has been shown that a proper selection of DSR parameters allows improvement of the mechanical property anisotropy of these materials. Jin and Lloyd[15] showed that an introduction of additional shear components (a so-called γ-fiber $\{1\ 1\ 1\}//ND$ in Euler angles space) to the deformation texture of AA5754 aluminum alloy also prominently affects the recrystallization texture formed during subsequent heat treatment. The presence of γ-fiber inhibits the growth of the undesired $\{0\ 0\ 1\}\langle 100\rangle$ cubic component, which is recognized as the main reason for low susceptibility to deep drawing of aluminum alloys designed for car body applications. On the other hand, Lee *et al.*[16] reported that the DSR process not only enhances the plasticity of AZ31 magnesium alloy as compared to conventional rolling but also leads to a simultaneous improvement of in-plane isotropy through facilitating the activation of prismatic slip during deformation.

In the present article, existing experimental data are supplemented with the results of our electron backscatter diffraction (EBSD) examination of the microstructure, the texture, and the internal lattice strain evolution of Armco iron during DSR processing.

II. EXPERIMENTAL DETAILS

A. *Material Processing*

Commercially pure Fe Armco samples in the form of rectangular plates with dimensions of 25 × 10 × 150 mm (width × thickness × length) were subjected to a preliminary thermomechanical treatment, which included cold rolling to 80 pct of a thickness reduction followed by 1-hour recrystallization annealing at 700 °C. This treatment allows obtainment of fully recrystallized material with a fine-grained structure. Such prepared samples were subsequently processed by main cold rolling to 85 pct of cold work. The final thickness reduction of 85 pct was obtained in two consecutive rolling passes. In the first pass, the reduction was 50 pct (from 2- to 1-mm thickness), and in the second pass, it was 70 pct (from 1 to 0.3 mm). The samples were 180 deg rotated along their normal axis (“back and forth”) between rolling passes. It was previously shown[17,18] that this kind of alteration of deformation path (due to a change of the shear strain direction between consecutive processing operations) is beneficial in terms of enhancing the grain refinement effect and, thus, improving the mechanical properties of processed material.

The deformation process was carried out on a sexton-type rolling mill equipped with working rolls made of tungsten carbide, with an equal diameter of 85 mm. In the present work, the cold rolling process was conducted in the following variants involving different values of the roll speed differentiation parameter R:

(1) rolling with equal velocity of both rolls (2 m/min) (further referred to as normal rolling, $R = 1$), and
(2) DSR with a constant velocity of the upper roll (2 m/min) and a different velocity of the lower one: 2, 3, and 4 times smaller (further marked as $R = 2$, 3, and 4, respectively).

B. *Material Characterization*

The EBSD system coupled with an FEI Quanta 3D field emission gun–scanning electron microscope was applied in order to analyze the microstructure, the microtexture, and the lattice strain evolution in the cold-deformed Fe samples. Before the examination, all samples were sub-

jected to a careful metallographic preparation routine (grinding with 120- to 4000-SiC papers, polishing with 3- to 0.25-μm diamond suspensions, and final polishing with 0.1- to 0.06-μm silica suspensions) in order to minimize the negative effects of the surface condition on acquired diffraction data. The EBSD investigation was carried out on the middle part of the longitudinal sections of rolled samples (in the rolling direction–normal direction (RD–ND) plane). For each sample, data were acquired from an area that was approximately 150 × 150 μm in size for a step size of 0.6 μm (for a textural analysis) and from an area of 15 × 15 μm in size for a step size of 0.06 μm (for a more detailed microstructural analysis). Several scans were performed for each sample, and then representative examples were chosen for publication. Acquired data were analyzed using TSL OIM Analysis 5 commercial software. Evaluation of a grain boundary distribution was made with an assumption of 2 to 15 deg misorientation angle for low-angle grain boundaries (LAGBs) and above 15 deg for HAGBs. Due to the presence of an "orientation noise" in heavily deformed samples, a software cleaning routine of as-received diffraction data was applied; points with neighbor-to-neighbor confidence index values lower than 0.2 were excluded from the analysis.[19] A quantitative microstructural analysis was conducted according to definitions proposed in the work of Jazaeri and Humphreys,[20] where a subgrain size was defined as an average LAGB spacing measured both in the normal and rolling directions and lamellar boundary (LB) spacing as HAGB intercepts measured in the ND.

The EBSD method was additionally applied to analyze lattice strain introduced into the material during plastic deformation by analyzed rolling techniques. Principles of the EBSD lattice strain assessment have been described elsewhere (*e.g.*, in our previous works[21],[22]). In the present work, diffraction pattern quality deterioration and local misorientation analysis approaches[23],[24] were chosen.

EBSD microtextural analysis was conducted by orientation distribution function (ODF) calculations using the Harmonic Series Expansion method, assuming both cubic crystal symmetry and an orthonormal (for the initial material) or a triclinic (for all rolled specimens) symmetry of the sample. The analysis was conducted in an extended Euler angle space ($\varphi_1 = 0 \div 360$ deg, $\Phi = 0 \div 90$ deg, and $\varphi_2 = 0 \div 90$ deg).

In order to analyze the effect of applied cold rolling variants on the change of mechanical properties of the investigated material, Vickers microhardness measurements were conducted on longitudinal sections of samples using a 100-g load and a 15-seconds loading time for a single measurement (15 measurements were performed for each sample, which were used to calculate average values and standard deviations).

III. RESULTS AND DISCUSSION

A. *Microstructure Evolution*

The Armco iron in its initial state (after preliminary thermomechanical treatment) has a fully recrystallized microstructure with an average grain size of ~6 μm (Figure 1). Cold rolling by all considered variants leads to an intensive microstructural evolution. Figures 2 and 3 show EBSD inverse pole figure maps of Fe samples in their initial state and after cold rolling with different R parameter values. Typical for cold-rolled metals, lamellar structures consisting of elongated boundaries and short interconnecting boundaries are observed (Figure 2). Moreover, extremely fine subgrains and grains are found for samples deformed with a high ratio of roll speed differentiation (*i.e.*, $R = 3$ and $R = 4$; Figures 3(d) and (e), respectively). Since the size of these grains is much lower (below 1 μm) than that of the initial grains, it is reasonable to assume that some processes of strain-assisted grain refinement take place upon these rolling variants.

It was shown by Hughes and Hansen[25] that a strain-induced structure evolution upon cold rolling involves subdivision of initial grains on "microvolumes" separated by LAGBs or HAGBs. With the rise in deformation degree, average spacing (a distance) between adjacent boundaries of both types decreases with a simultaneously observed increase of the misorientation angle. Results of a transmission electron microscopy evaluation show that the deformed, subdivided structure of metals is composed of small dislocation-free regions (cells) arranged in blocks and surrounded by dislocation walls. Upon increasing the imposed strain, the structure undergoes further transformation, which includes internal rotations in deformation bands leading to the formation of new grains. On the other hand, an alternative mechanism of structure refinement during DSR processing of dual-phase low carbon steel was proposed in the recent work of Hamad *et al.*[26] The authors concluded that the formation of fine grains located along deformation band boundaries (a so-called

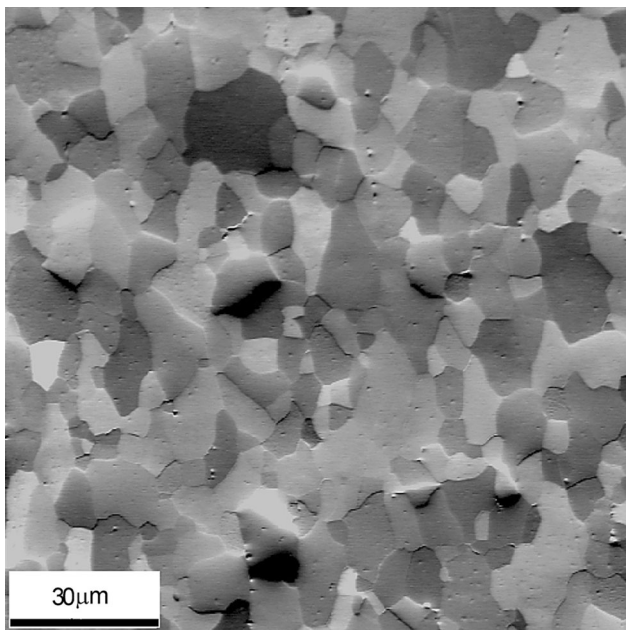

Fig. 1—SEM microphotograph of Fe Armco in its initial state.

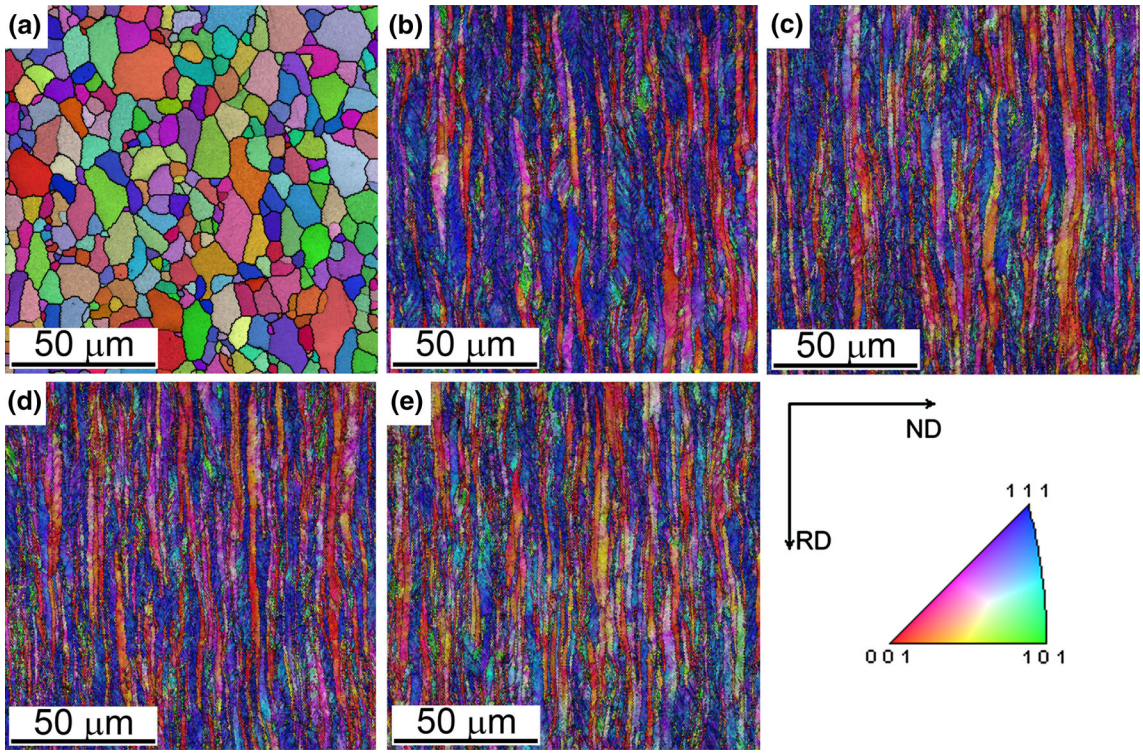

Fig. 2—EBSD inverse pole figure maps taken at a "low magnification" from iron samples in (*a*) an initial state and after cold rolling to 85 pct with (*b*) $R = 1$, (*c*) $R = 2$, (*d*) $R = 3$, and (*e*) $R = 4$.

"necklace" structure) is an effect of a continuous dynamic recrystallization process. This process is based on the strain-activated coalescence of subgrains inside deformed elongated grains, which leads to a transfiguration of LAGBs into HAGBs. The fraction of grains with size below 1 μm was also found to increase with the increasing number of DSR operations.

The EBSD images presented in Figure 3 confirm a decrease of boundary spacing with the rising value of the R parameter; thus, it may be concluded that, for all DSR variants of rolling ($R = 2 \div 4$), a higher strain was introduced into the material than in the case of rolling with equal speed of both rolls ($R = 1$).

The results of the quantitative microstructural analysis are presented in Figure 4. It is found (Figure 4(a)) that the average distance between adjacent lamellar boundaries is nearly two times (for the $R = 2$) and 3 times (for the $R = 3$ and the $R = 4$) smaller than for the sample rolled with an equal speed of both rolls. Values of the LB spacing are far below 1 μm for all DSR-processed samples. A similar trend was also observed for the subgrain size calculated as an average LAGB spacing. The results of grain size diameter distribution presented in Figure 4(b) confirm a structural refinement during the DSR processing of iron; the fraction of grains with the submicron size increases upon raising the R value, reaching ~70 pct for the highest considered value of the R parameter. These results are similar to those presented by Hamad *et al.*[14] However, since some fraction of these grains (~40 pct) is also found in the sample cold deformed with an equal speed of both rolls, the obtained results imply that the differentiation of the roll speed results with a triggering of some additional phenomenon. According to the results shown by Megantoro *et al.*,[27] an application of DSR processing leads to a prominent temperature rise in an IF steel sample. It was shown that the temperature rise increases with an increase in either the thickness reduction or the roll speed ratio, approaching a maximum value of 373 K (100 °C) under the thickness reduction of 40 pct and a roll speed ratio of 1:4. Since, in the present study, the reduction per pass was even higher (50 and 70 pct in the first and second rolling passes, respectively), it may be assumed that the generated heat was also higher. However, in the present case of cold rolling of Armco iron, the temperature rise of 100 °C (or even higher) is too low to activate a dynamic recrystallization process. Nevertheless, the results of microstructural examination revealed that an application of the high roll speed mismatch (the $R = 4$) leads to both a decrease of boundary spacing and a formation of a well-developed subgrain structure inside the deformation bands. These findings are similar to those presented by Valiev *et al.*,[28] who concluded that high plastic straining leads to an increase in the number of dislocations that are known to concentrate in cell walls. The decrease of dislocation wall thickness, and thus the increase of cell size, is usually attributed to the recovery process, which permits segment rearrangements. Thus, it seems to be more reasonable to call the observed structure evolution a subgrain structure evolution through accumulated shear deformation, which may be related to the dynamic recovery process. Since the observed structural changes take place inside deformation bands, and do

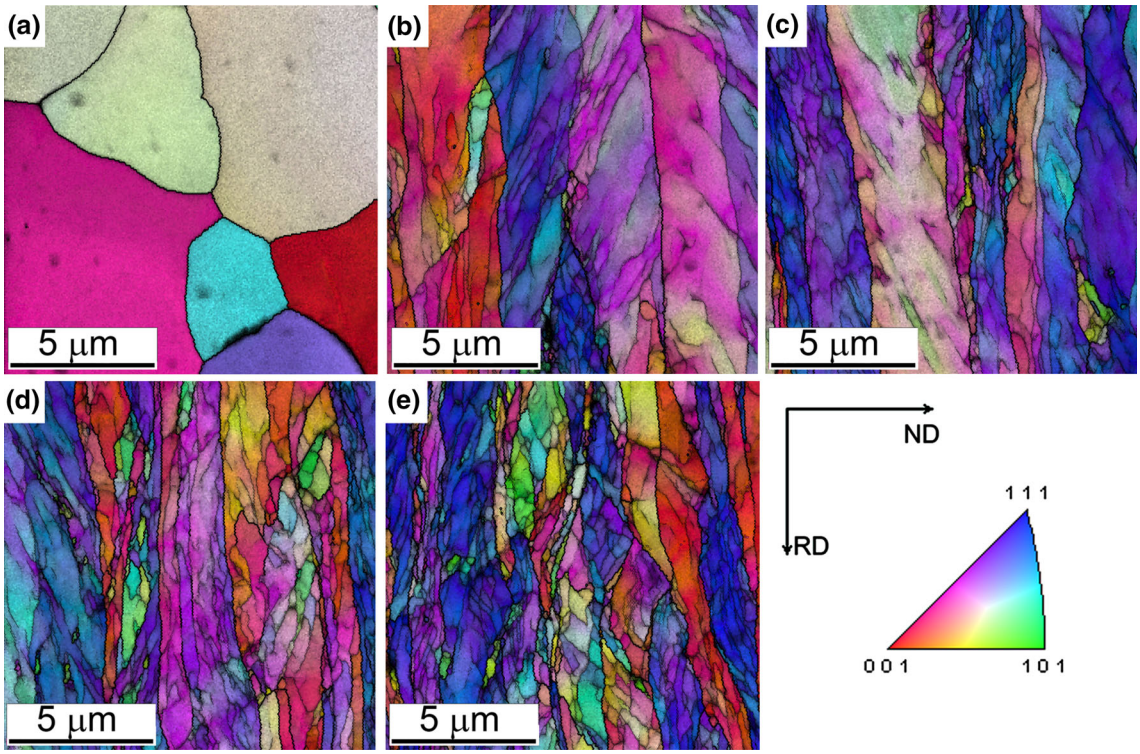

Fig. 3—EBSD inverse pole figure maps taken at a "high magnification" from iron samples in (*a*) an initial state and after cold rolling to 85 pct with (*b*) $R = 1$, (*c*) $R = 2$, (*d*) $R = 3$, and (*e*) $R = 4$. HAGBs are marked with thick lines.

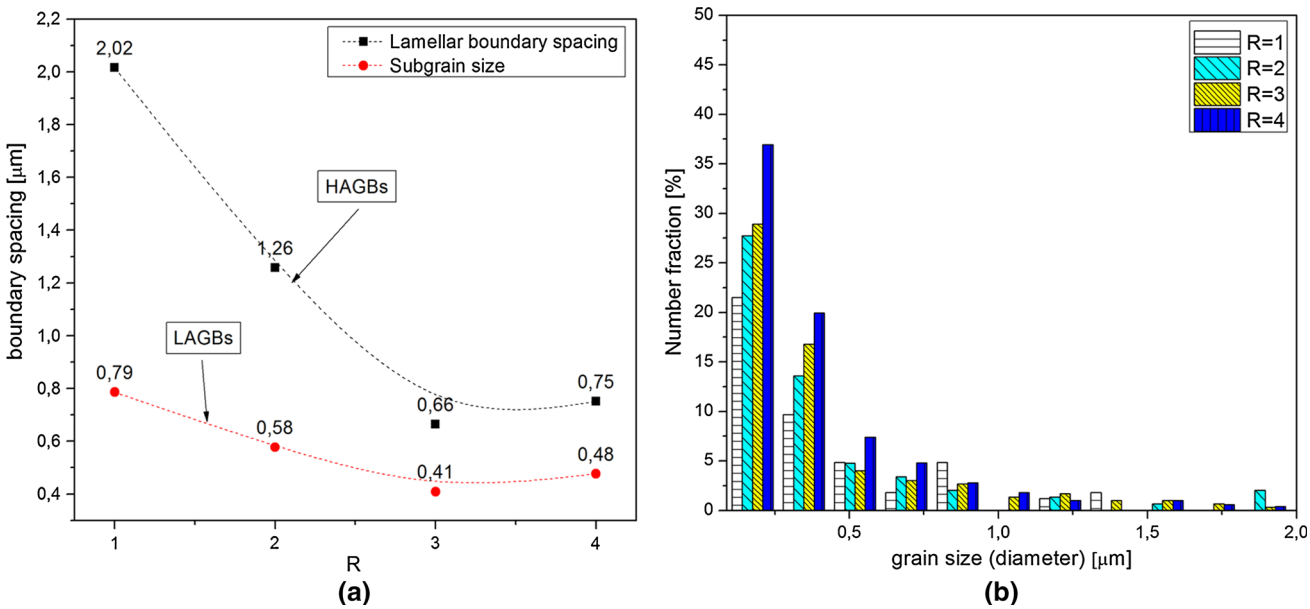

Fig. 4—(*a*) Boundary spacing plotted as a function of the *R* value. (*b*) Grain size (diameter) distribution diagram for the 85 pct cold-rolled iron with different values of the *R* parameter.

not lead directly to the formation of a fully equiaxed grain structure, it may be stated that a high fraction of submicron grains in the material subjected to the high ratio DSR method is an effect of both the strain-induced grain subdivision and the temperature rise, which supports activation of the continuous dynamic recovery and shear-assisted substructure rearrangement.

B. *Microtexture Evolution*

Cold rolling of bcc metals and alloys results in a formation of deformation texture that is composed of few orientation fibers, among which the most important are the α-fiber and the γ-fiber, both located in the $\varphi_2 = 45$ deg section of the Euler angle space (Figure 5). The

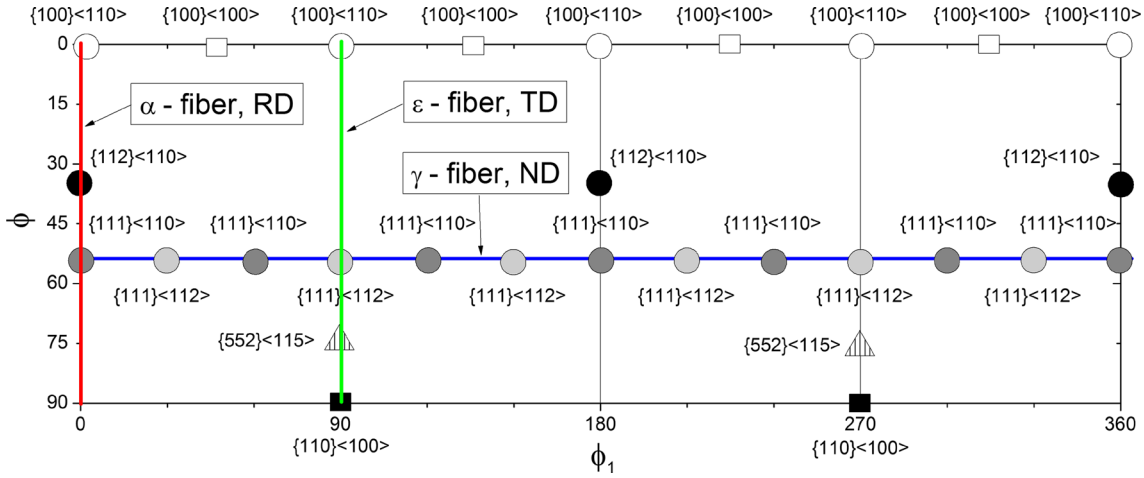

Fig. 5—Nominal positions of texture components in the $\varphi_2 = 45$ deg section of the Euler space.

former fiber contains orientations that have ⟨110⟩ directions parallel to the RD (and is also called an *RD fiber*). The latter one connects orientations with {111} planes parallel to the rolling plane (and for a cubic crystal may be described also as an *ND fiber*).[29]

Figure 6 shows $\varphi_2 = 45$ deg sections of the Euler space obtained for the material in its initial state and after cold rolling to 85 pct thickness reduction with different values of the R parameter. It is found (Figure 6(a)) that material in its initial state exhibits a weak texture with the {100}⟨100⟩ component and some residual (after the previous thermomechanical treatment) trace of the γ-fiber. Cold rolling to 85 pct thickness reduction by all proposed variants leads to a formation of rolling texture that is composed of the aforementioned fibers.

The material deformed without roll speed differentiation ($R = 1$, Figure 6(b)) shows a typical bcc metal rolling texture characterized by a well-developed γ-fiber (with a special emphasis on a {111}⟨112⟩ orientation) and an α-fiber dominated by a {100}⟨110⟩ component. By analyzing the results presented in Figures 6(c) through (e), it may be concluded that the DSR processing of iron results in an overall texture weakening effect and a displacement of both the α-fiber and γ-fiber. The effect of the aforementioned fiber deterioration due to an introduction of shear deformation into the rolling process was also noted in the recent work by Tóth *et al.*[30] The authors, using the viscoplastic slip and the Taylor model-based calculations, found that both the RD and the ND fibers are strongly affected by deformation mode and are completely unstable for simple shear. In this attempt, the lack of texture component (or a fiber) stabilization means that, under an imposed deformation gradient, its rotation rate is nonzero and may move to some different, more stable orientation. It was previously shown[31] that the deformation gradient in the DSR method is approximated by a superposition of a plane strain (which is specific for the normal rolling process) and a simple shear in the rolling direction (Eq. [1]). Additionally, the impact of the simple shear component (ε_{xz}) rises with an increase in the R parameter, leading to an accumulation of a higher strain.

$$\varepsilon_{ij} = \begin{bmatrix} \varepsilon_{xx} & 0 & 0 \\ 0 & 0 & 0 \\ 0 & 0 & \varepsilon_{zz} = -\varepsilon_{xx} \end{bmatrix} + \begin{bmatrix} 0 & 0 & \varepsilon_{xz} \\ 0 & 0 & 0 \\ 0 & 0 & 0 \end{bmatrix} = \begin{bmatrix} \varepsilon_{xx} & 0 & \varepsilon_{xz} \\ 0 & 0 & 0 \\ 0 & 0 & \varepsilon_{zz} = -\varepsilon_{xx} \end{bmatrix} \quad [1]$$

Plane strain (normal rolling) *Simple shear* *Complex state (DSR)*

This effect of a progressive shifting of the main orientation fibers from their nominal positions with the increasing R value is confirmed by fiber plots calculated for their "ideal course" (Figure 7). It may be found that, due to the displacement of fibers in the Euler space, calculated ODF values in the exact positions of each fiber are lowered with the rise in R parameter values. This fact is prominently visible in the run of the γ-fiber (Figure 7(b)) for the $R = 4$ sample, which exhibits only marginal ODF values that are even lower than those calculated for the material before rolling. However, samples cold rolled with high roll speed mismatch ($R = 3$ and $R = 4$), despite overall lower values of calculated ODFs, exhibit strong peaks near {111}⟨1-21⟩ and {111}⟨-211⟩ locations, respectively,

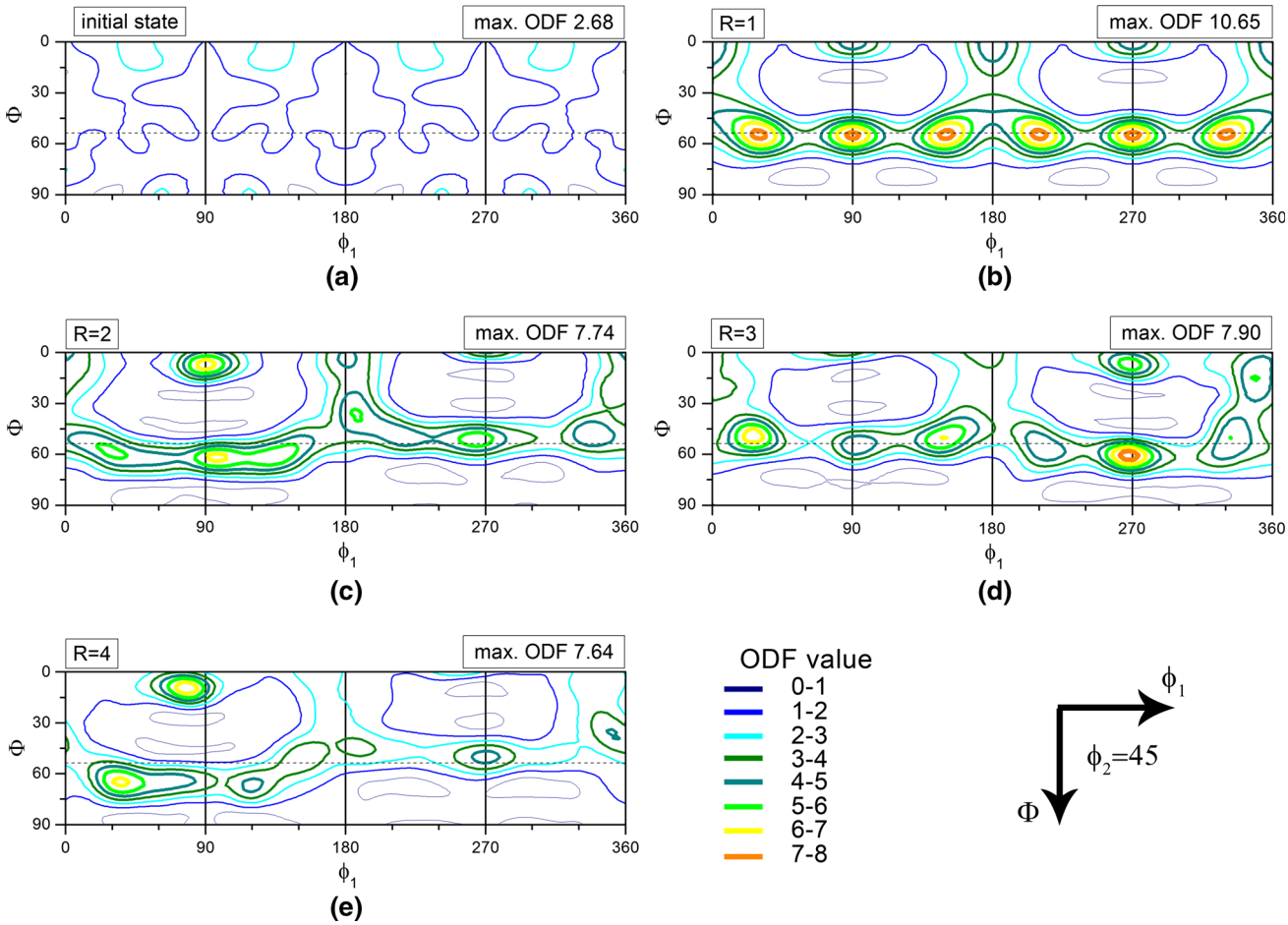

Fig. 6—Crystallographic texture represented in $\varphi_2 = 45$ deg sections of the Euler space obtained for the material in its initial state and after cold rolling to 85 pct of thickness reduction with a different value of the *R* parameter.

indicating that these positions are preferably stable under imposed shear deformation. The obtained results showing texture fibers "blurring" are also in good agreement with those presented by Hamad *et al.*,[14] where a crystallographic texture of the DSR-processed IF steel was characterized as typical for cold-rolled bcc metal orientations without traces of any additional shear components. Thus, it is reasonable to state that the DSR processing of iron leads to a shifting of normal rolling texture components, rather than to a formation of completely new ones.

C. *Strain Changes During Rolling*

An evaluation of strain introduced during cold rolling was carried out by means of microhardness measurements and EBSD lattice strain analysis. The results of microhardness measurements are shown in Figure 8(a). It is found that cold rolling to 85 pct thickness reduction by each considered deformation method leads to a significant strain hardening effect. However, the DSR processed samples exhibited a distinctly higher hardness than the normally rolled sample ($R = 1$). Moreover, a decrease of calculated standard deviation values upon raising the roll speed mismatch confirms a more homogeneous course of deformation with the presence of additional shear strain. This finding is in line with the results of previously reported works on various DSR-processed materials (*e.g.*, Al[32] and Cu[11]) and may be related to a decrease in surface frictional stresses (which are cited as the main reason for the nonuniformity of deformation upon rolling[33]) with a rise in roll speed mismatch.

The microhardness measurements were also supplemented by the EBSD strain assessment conducted by both image quality (IQ) analysis and local misorientation analysis represented by a grain orientation spread (GOS) parameter. One of the most important conditions of receiving valuable results from the IQ analysis is a careful and repeatable surface preparation of analyzed samples. Thus, we have paid special attention to the sample preparation process in order to exclude its possible effect on the obtained results. To the best of our knowledge, the results presented in this article are free from disruptions from surface defects. In this analysis, the quality of the obtained diffraction pattern is assumed to be significantly affected by the crystal lattice quality (*e.g.*, the density of lattice defects). It was shown that the lattice strain introduced during plastic deformation leads to a higher fuzziness of the Kikuchi diffraction patterns (and, thus, shifting the IQ histogram to lower values). The basis of the method is a comparative analysis of the IQ histograms of

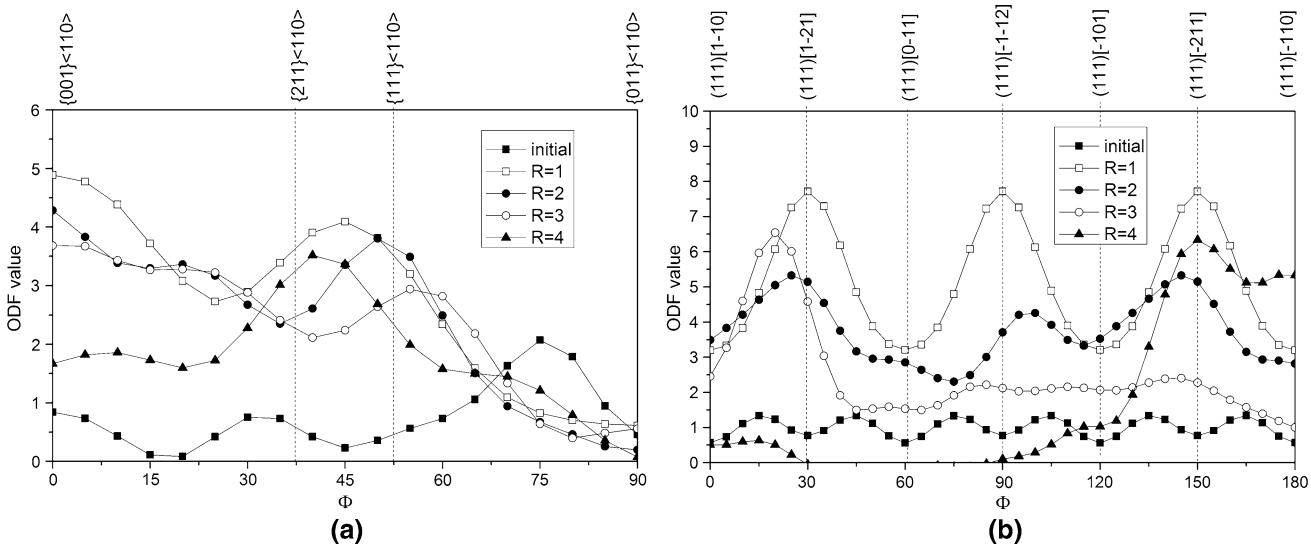

Fig. 7—ODF fiber plots calculated in their "ideal positions" for iron in its initial state and after different variants of cold rolling: (*a*) the α-fiber plots and (*b*) the γ-fiber plots.

two samples: one sample is fully recrystallized, and the other sample is deformed to some strain value (the principle of the method is graphically presented in Figure 8(b)). This comparative study allows for an extraction of these points, which belong to deformed or undeformed volumes of the material, respectively. To associate the experimental IQ values with the introduced strain, the normalized IQ histograms are separated into deformed (region A in Figure 8(b)) and undeformed (region B in Figure 8(b)) material volumes. However, some points included in the histograms (region C in Figure 8(b)), which are common to both distributions, could not be unequivocally assigned to either the deformed or undeformed material. Thus, a minimum deformed fraction X_{min} and not a total deformed fraction of the analyzed sample could be estimated. The experimental reduced IQ histograms that were obtained for iron samples after different variants of deformation (Figure 8(c)) were used to calculate the minimum deformed fraction X_{min} (Figure 8(d)).

The second approach to the EBSD strain assessment involves an analysis of local misorienation changes. The principles of this method are based on an assumption of strain-assisted internal rotations of microvolumes (cells or subgrains) within grains, which means that a transmission and accommodation of a plastic strain result in an increase of internal GOS. Therefore, grains that undergo deformation (and, thus, are extensively defected) exhibit high GOS value, and reversely, those that are undeformed (defect free) have very low GOS values, close to zero.[34]

Interestingly, despite the observed higher hardness of DSR specimens, calculated changes of the X_{min} plotted as a function of the R parameter exhibited an inverse, negative, and almost linear trend (Figure 8(d)). Since this parameter is closely related to lattice defect density, it may be stated that, during rolling with an additional presence of shear strain (R = 2, 3, or 4), some part of the stored energy of deformation is released due to the activation of dynamic structure restoration processes (*e.g.*, a recovery). These results seem to be confirmed by the EBSD maps presented in Figure 4, which show the formation of cell-like substructural features for the sample rolled with the highest considered value of the roll speed ratio (R = 4, Figure 3(e)).

Results of the GOS-based analysis are shown in Figure 9. In our previous research, devoted to the EBSD study on recrystallization of cold-rolled Ni_3Al-based alloy,[22] we showed that the GOS-based analysis allows distinguishing grains that belong to the deformed matrix and those that undergo static recovery or recrystallization. GOS values below 1 deg and in the range of 1 to 3 deg were designated as newly formed (recrystallized) and recovered grains, respectively. In the present case, it was found that, since Armco iron in the initial condition, in its fully recrystallized state (Fig. 9a), is characterized by extremely low GOS values (mostly below 1 deg), cold deformation leads to a substantial increase and scattering of the orientation spread. Nevertheless, maps presented in Figure 9 reveal that some fine grains observed in the microstructure of cold-deformed samples also exhibit GOS values below 1 deg and up to 3 deg, which may be related to defect-free volumes, as previously stated. Moreover, a fraction of these grains as well as a fraction of HAGBs increases with the rise in roll speed mismatch (Table I). These results also support the possible activation of structure restoration phenomena upon DSR processing.

IV. CONCLUSIONS

Generally, application of the DSR process leads to higher strengthening of the investigated Fe Armco than does application of the conventional rolling process, as confirmed by the results of microhardness measure-

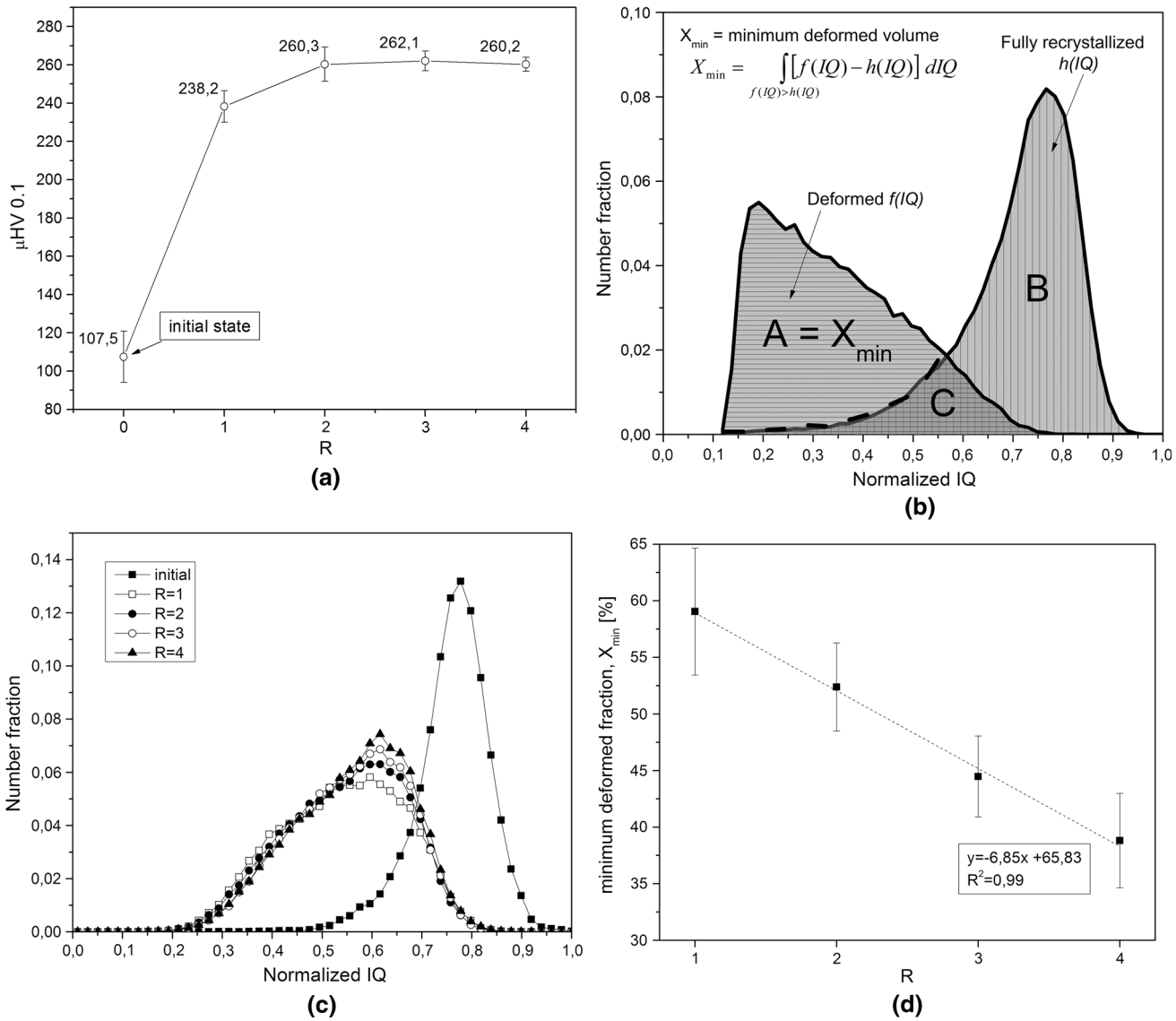

Fig. 8—(*a*) Microhardness plot as a function of the *R* parameter, (*b*) schematic of the strain assessment method using IQ histogram analysis,[23] (*c*) experimental reduced IQ histograms obtained for iron in its initial state and cold rolled with different values of the *R* parameter, and (*d*) plot of the calculated minimum deformed fraction as a function of the *R* parameter.

ments. Additionally, lower standard deviation values point to a more homogenous deformation course upon use of the DSR method. This strengthening effect results from structure refinement, which is a consequence of the DSR process; samples of iron processed with a high roll speed mismatch were characterized by a high fraction of grains with submicron size ~70 pct for the highest considered value of the *R* parameter. Based on the obtained experimental results and supported by appropriate data from the literature, it may be concluded that the structure refinement is an effect of both the shear strain-induced grain subdivision and the temperature rise, which supports activation of a subgrain evolution *via* continuous dynamic recovery. Results of the texture examination show that DSR processing of iron leads to an overall texture weakening and a displacement of bcc normal rolling texture components, rather than to a formation of completely new ones. Due to a change in the deformation gradient (an additional presence of a shear strain), main texture fibers undergo a shift to more stable positions. The results of EBSD lattice strain analysis show that, despite the higher hardness of the DSR samples, the estimated lattice strain (expressed as the minimum deformed fraction) decreases with an increase of the roll speed mismatch. This finding indicates that, upon the DSR process, some part of the storage energy of deformation is released due to a dynamic transformation of the material structure into a more stable state. However, since the observed structural changes take place inside deformation bands and do not lead directly to the formation of a fully equiaxed grain structure, it seems to be more reasonable to call

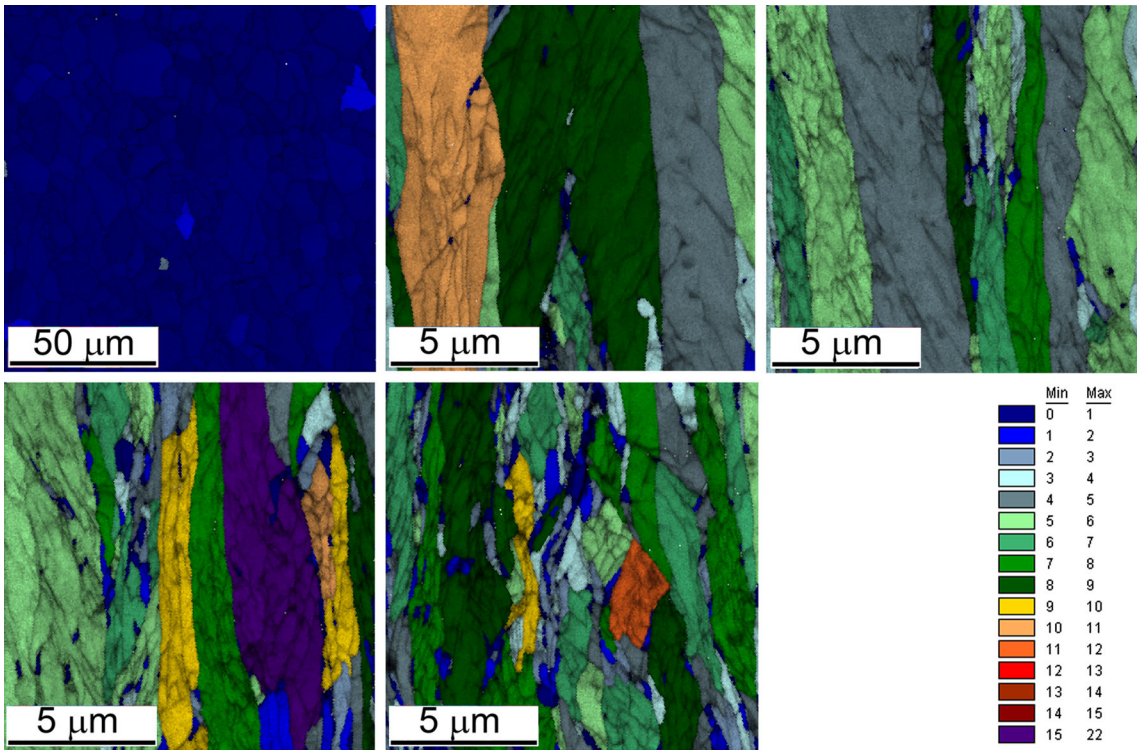

Fig. 9—EBSD grain orientation spread maps taken from iron samples in (*a*) an initial state and after cold rolling to 85 pct with (*b*) $R = 1$, (*c*) $R = 2$, (*d*) $R = 3$, and (*e*) $R = 4$. The color code is consistent with the respective GOS value ranges located on the right side of the figure.

Table I. Results of the GOS-Based EBSD Strain Assessment and HAGB Fraction Analysis

	GOS Fraction (Pct)				
R	0 to 1 deg	1 to 2 deg	2 to 3 deg	Σ 0 to 3	HAGBs Fraction (Pct)
0—initial	97.9	1.9	0.1	99.9	93
1	0.8	0.9	0.9	2.6	19.9
2	1.1	0.7	1.4	3.2	25.2
3	3.4	3.9	3.2	10.5	28.1
4	7.7	18.1	21	46.8	30.5

the observed structure transformation a subgrain structure evolution through accumulated shear deformation, which may be related to the dynamic recovery process.

ACKNOWLEDGMENT

The authors gratefully acknowledge the financial support from the Polish National Center of Science under Grant Nos. 2013/09/N/ST8/04366 and UMO-2011/01/B/ST8/07257.

OPEN ACCESS

REFERENCES

1. R.Z. Valiev, R.K. Islamgaliev, and I.V. Alexandrov: *Progr. Mater. Sci.*, 2000, vol. 45, pp. 103–89.
2. Y.T. Zhu, T.C. Lowe, and T.G. Langdon: *Scripta Mater.*, 2004, vol. 51, pp. 825–30.
3. R.Z. Valiev, R.K. Islamgaliev, and I.P. Semenova: *Mater. Sci. Eng. A*, 2007, vol. 463, pp. 2–7.
4. S.O. Moussa and M. Samy El-Shall: *J. Alloys Compd.*, 2007, vol. 440, pp. 178–88.
5. M. Richert, H.J. McQueen, and J. Richert: *Can. Metall. Q.*, 1998, vol. 37, pp. 449–57.
6. T. Sakai, H. Miura, A. Goloborodko, and O. Sitdikov: *Acta Mater.*, 2009, vol. 57, pp. 153–62.
7. Y. Estrin and A. Vinogradov: *Acta Mater.*, 2013, vol. 61, pp. 782–817.
8. F. Zuo, J. Jiang, A. Shan, J. Fang, and X. Zhang: *Trans. Nonferrous Met. Soc. China*, 2008, vol. 18, pp. 774–77.
9. H.S. Kim, S.J. Yoo, J.W. Ahn, D.H. Kim, and W.J. Kim: *Mater. Sci. Eng. A*, 2011, vol. 528, pp. 8479–85.
10. W.J. Kim, H.G. Jeong, and H.T. Jeong: *Scripta Mater.*, 2009, vol. 61, pp. 1040–43.
11. W. Polkowski, P. Jóźwik, M. Polański, and Z. Bojar: *Mater. Sci. Eng. A*, 2013, vol. 564, pp. 289–97.
12. W. Polkowski, P. Jóźwik, and Z. Bojar: *Mater. Lett.*, 2015, vol. 139, pp. 46–49.

13. J. Suharto and Y.G. Ko: *Mater. Sci. Eng. A*, 2012, vol. 558, pp. 90–94.
14. K. Hamad, B.K. Chung, and Y.G. Ko: *Mater. Charact.*, 2014, vol. 94, pp. 203–214.
15. H. Jin and D.J. Lloyd: *Mater. Sci. Eng. A*, 2005, vol. 399, pp. 358–67.
16. J.B. Lee, T.J. Konno, and H.G. Jeong: *J. Alloys Compd.*, 2010, vol. 499, pp. 273–77.
17. Y.G. Ko, C.S. Lee, D.H. Shin, and S.L. Semiatin: *Metall. Mater. Trans. A*, 2006, vol. 37A, pp. 381–91.
18. L.L. Chang, S.B. Kang, and J.H. Cho: *Mater. Des.*, 2013, vol. 44, pp. 144–48.
19. A.J. Schwartz, M. Kumar, B.L. Adams, and D. Field: *Electron Backscatter Diffraction in Materials Science*, 2nd ed., Springer, New York, 2009.
20. H. Jazaeri and F.J. Humphreys: *Acta Mater.*, 2004, vol. 52, pp. 3239–50.
21. W. Polkowski, P. Jóźwik, K. Karczewski, and Z. Bojar: *Arch. Civ. Mech. Eng.*, 2014, vol. 14, pp. 550–60.
22. W. Polkowski, P. Jóźwik, and Z. Bojar: *J. Alloys Compd.*, 2014, vol. 614, pp. 226–33.
23. J. Tarasiuk, P. Gerber, and B. Bacroix: *Acta Mater.*, 2002, vol. 50, pp. 1467–77.
24. S. Wroński, J. Tarasiuk, B. Bacroix, A. Baczmański, and C. Braham: *Mater. Character.*, 2012, vol. 73, pp. 52–60.
25. D.A. Hughes and N. Hansen: *Acta Mater.*, 1997, vol. 45, pp. 3871–86.
26. K. Hamad, R.B. Megantoro, and Y.G. Ko: *J. Mater. Sci.*, 2014, vol. 49, pp. 6608–19.
27. R.B. Megantoro and Y.G. Ko: *J. Alloys Compd.*, 2014, vol. 586, pp. S254–S257.
28. R.Z. Valiev, Y.V. Ivanisenko, E.F. Rauch, and B. Baudelet: *Acta Mater.*, 1996, vol. 44, pp. 4705–12.
29. O. Engler and V. Randle: *Introduction to Texture Analysis: Macrotexture, Microtexture and Orientation Mapping*, 2nd ed., Taylor and Francis Group, Boca Raton, 2010.
30. L.S. Tóth, B. Beausir, D. Orlov, R. Lapovok, and A. Haldar: *J. Mater. Process. Technol.*, 2012, vol. 212, pp. 509–15.
31. J. Sidor, A. Miroux, R. Petrov, and L. Kestens: *Acta Mater.*, 2008, vol. 56, pp. 2495–2507.
32. Y.G. Ko: *J. Alloys Compd.*, 2012, vol. 536, pp. S122–S125.
33. Y.G. Ko, J. Suharto, J.S. Lee, B.H. Park, and D.H. Shin: *Met. Mater. Int.*, 2013, vol. 19, pp. 603–09.
34. F.J. Humphreys: *J. Mater. Sci.*, 2001, vol. 36, pp. 3833–54.